



# HHS Public Access

Author manuscript

*J Biomech.* Author manuscript; available in PMC 2017 October 03.

Published in final edited form as:

*J Biomech.* 2016 October 3; 49(14): 3200–3207. doi:10.1016/j.jbiomech.2016.07.036.

## Quantifying Achilles Tendon Force *In Vivo* from Ultrasound Images

Taylor JM. Dick<sup>1,\*</sup>, Allison S. Arnold<sup>2</sup>, and James M. Wakeling<sup>1</sup>

<sup>1</sup>Department of Biomedical Physiology and Kinesiology, Simon Fraser University, Burnaby, BC, Canada

<sup>2</sup>Concord Field Station, Harvard University, Bedford, MA, USA

### Abstract

This study evaluated a procedure for estimating *in vivo* Achilles tendon (AT) force from ultrasound images. Two aspects of the procedure were tested: (i) accounting for subject-specific AT stiffness and (ii) accounting for changes in the relative electromyographic (EMG) intensities of the three triceps surae muscles. Ten cyclists pedaled at 80 r.p.m. while a comprehensive set of kinematic, kinetic, EMG, and ultrasound data were collected. Subjects were tested at four crank loads, ranging from 14 to 44 N·m (115 to 370 W). AT forces during cycling were estimated from AT length changes and from AT stiffness, which we derived for each subject from ultrasound data and from plantar flexion torques measured during isometric tests. AT length changes were measured by tracking the muscle-tendon junction of the medial gastrocnemius (MG) relative to its insertion on the calcaneus. Because the relative EMG intensities of the triceps surae muscles varied with load during cycling, we divided subjects' measured AT length changes by a scale factor, defined as the square root of the relative EMG intensity of the MG, weighted by the fractional physiological cross-sectional areas of the three muscles, to estimate force. Subjects' estimated AT forces during cycling increased with load ( $p < 0.05$ ). On average, peak forces ranged from  $920 \pm 96$  N (14 N·m, 115 W) to  $1510 \pm 129$  N (44 N·m, 370 W). For most subjects, ankle moments derived from the ultrasound-based AT strains were 5 to 12% less than the net ankle moments calculated from inverse dynamics ( $r^2 = 0.71 \pm 0.28$ , RMSE =  $8.1 \pm 0.33$  N·m). Differences in the moments increased substantially when we did not account for changes in the muscles' relative EMG intensities with load or, in some subjects, when we used an average stiffness, rather than a subject-specific value. The proposed methods offer a non-invasive approach for studying *in vivo* muscle-tendon mechanics.

\* Corresponding author (taylor\_dick@sfu.ca), Telephone: 778-782-8445, Fax: 778-782-3040.

**Publisher's Disclaimer:** This is a PDF file of an unedited manuscript that has been accepted for publication. As a service to our customers we are providing this early version of the manuscript. The manuscript will undergo copyediting, typesetting, and review of the resulting proof before it is published in its final citable form. Please note that during the production process errors may be discovered which could affect the content, and all legal disclaimers that apply to the journal pertain.

All authors were directly involved in the preparation and execution of this study. All authors contributed to the writing of the manuscript. The material in this manuscript will not be submitted for publication elsewhere.

Conflict of interest statement

There are no conflicts of interest.

## Keywords

ultrasound; tendon stiffness; muscle force; ankle moment

---

## Introduction

The purpose of this study was to evaluate a procedure for estimating Achilles tendon (AT) forces from ultrasound-based measurements of AT length changes. Over the past decade, B-mode ultrasound has emerged as a useful tool for quantifying *in vivo* muscle-tendon parameters during movement. For example, ultrasound images of muscle fascicles have been recorded during walking, running (Lichtwark and Wilson 2006; Farris and Sawicki, 2012), and jumping (Kurokawa et al., 2001) and have been used to quantify fascicle strains. Ultrasound has also been used, with motion capture, to measure mechanical properties of tendons under isometric conditions (Kongsgaard et al., 2011) and during walking (Lichtwark and Wilson, 2006) and hopping (Lichtwark and Wilson, 2005). These and other studies (e.g., Maganaris, 2003) have shown that ultrasound-based approaches can provide measures of muscle-tendon mechanics that cannot be obtained from motion capture alone.

Ultrasound-based measures of AT length changes, combined with information about the tendon's stiffness and slack length, could provide information about AT forces during dynamic tasks. For example, Lichtwark and Wilson (2006) estimated the average AT force generated by six subjects during walking by multiplying the subjects' average AT length changes, measured via ultrasound, by an average tendon stiffness that was estimated in a prior study (Lichtwark and Wilson, 2005). However, determining the forces transmitted by a complex, composite tendon such as the AT – in individual subjects – remains challenging for several reasons. First, AT stiffness has been shown to vary across subjects (Magnusson et al., 2001; Kubo et al., 2003; Lichtwark and Wilson, 2005; Morrison et al., 2015), and whether an average stiffness is sufficient to estimate force, or whether stiffness must be estimated on a per subject or per muscle basis, remains unknown. Second, three large muscles insert into the AT, and the relative contributions of the medial and lateral gastrocnemius (MG, LG) and soleus (SOL) to AT force may change, depending on the task (e.g., Wakeling and Horn, 2009; Wakeling et al., 2010). Thus, strains measured at a single muscle-tendon junction (MTJ) may not be representative of strains throughout the tendon (Franz et al., 2015). Third, AT strains that are calculated from measured length changes depend, in part, on the assumed slack length of the composite tendon; however, determining the AT's *in vivo* length at the start of force transmission is often not straightforward.

Our procedure extends previous approaches in two ways: it characterizes AT stiffness on a subject-specific basis, and it accounts for changes in the relative electromyographic (EMG) intensities of the MG, LG, and SOL. To evaluate the procedure, we asked 10 competitive cyclists to pedal at a steady 80 r.p.m. cadence at 4 different crank loads while we collected a comprehensive set of kinematic, kinetic, EMG, and ultrasound data. Cycling offers a unique paradigm for characterizing AT mechanics and testing new methods because loads can be varied to impose changes in the required joint moments without imposing large changes in the excursions of muscle-tendon units (MTUs). Here we estimate the forces and moments

transmitted by the AT during cycling. We compared these estimates to subjects' net ankle moments calculated from inverse dynamics, and assessed the sensitivity of these estimates to measured values of AT stiffness, AT slack length, and relative EMG intensities of MG, LG, and SOL. Our results provide important considerations for estimating AT forces from ultrasound images.

## Methods

### Acquisition of Experimental Data

Data were recorded from ten competitive female cyclists (age  $28 \pm 6$  years; Suppl. Table S1) recruited from local cycling clubs. Each test session included a cycling protocol, during which subjects pedaled on a stationary bicycle (Indoor Trainer, SRM, Julich, Germany), and an isometric protocol, during which subjects generated ankle plantar flexion moments while secured in a custom frame (Figs. 1 and 2). All subjects gave informed consent, and protocols were approved by Institutional Review Boards at Simon Fraser University and Harvard University.

During the cycling protocol, we recorded ultrasound images of the MG MTJ, the 3D trajectories of 32 LED markers, reaction forces effective and ineffective (normal and radial) to the crank, and surface EMG patterns from 10 muscles (Fig. 1A and Suppl. Fig. S1). A B-mode ultrasound probe (7MHz, 60mm field-of-view; Echoblaster, Teled, Vilnius, Lithuania) was secured over the distal MG MTJ on the right limb using a stretchy adhesive bandage, and an ultrasound gel pad (Parker Laboratories, NJ, USA) was placed at the probe-skin interface to enhance image quality and allow the muscles to bulge. We tracked the MTJs of both gastrocnemii in these experiments, but because the architecture of the MG is less complex than that of the LG (e.g., Wolf et al., 1998), we measured length changes of the AT at the MG MTJ (Suppl. Video S1), consistent with previous studies (e.g., Maganaris and Paul, 1999; Muramatsu et al., 2001). Markers were placed bilaterally over the greater trochanter, lateral epicondyle, lateral malleolus, calcaneus, and fifth metatarsal. Five markers were positioned on the pelvis, two were fixed on each pedal, and rigid marker triads were secured to the right thigh, shank, and ultrasound probe. Six "virtual" markers were defined based on the measured marker motions, segment lengths, and known bike dimensions; these markers located the subjects' hip centers (Siston and Delp, 2006), lateral epicondyles, and pedal centers of pressure. Markers were tracked at 100Hz using an optical motion capture system (Certus Optotrak, NDI, Waterloo, Canada). Ultrasound images were recorded at 40Hz, and prior calibration (Prager et al., 1998) determined the position of the ultrasound scanning plane relative to markers on the probe. While pedaling, subjects wore sport sandals with cleats that were secured to clipless instrumented pedals (Powerforce, Radlabor, Freiburg, Germany); the sandals had a stiff sole and allowed markers on the ankle and foot to be placed directly over bony landmarks on the skin. Reaction forces at the crank were recorded bilaterally at 2000Hz. On the left limb, bipolar Ag/AgCl surface EMG electrodes (10mm diameter, 21mm spacing; Norotrode; Myotronics, Kent, USA) were placed over the mid-bellies of the MG, LG, SOL, tibialis anterior (TA), and six other muscles (not reported here). EMG signals were preamplified (gain 1000), band-pass filtered (bandwidth 10–

500Hz; Biovision, Wehrheim, Germany), and sampled at 2000Hz as described elsewhere (e.g., Wakeling and Horn, 2009; Blake and Wakeling, 2015).

Subjects were tested at 11 combinations of cadence and crank torque. For this study, we analyzed trials in which subjects pedaled at 80 r.p.m. at crank torques of 14 (easy), 26, 35, and 44N·m (equivalent to a steep hill), corresponding to crank powers of 115, 220, 290, and 370W. Sets of trials, each 15s in duration, were repeated in random order following a 5min warm-up. “Maximum effort” sprint trials (high power and cadence) were collected at the beginning and end of each session in an effort to elicit maximum muscle activity; we used these data as a reference when normalizing the muscles’ EMG intensities (e.g., Rouffet and Hautier, 2008). Static calibration trials were collected in cycling posture to scale a musculoskeletal model to each subject (Fig. 1C), and dynamic hip range-of-motion trials were collected to help locate subjects’ hip centers. Between trials, subjects were encouraged to rest up to 30s. We confirmed that fatigue was not a factor by comparing EMG data collected at the beginning and end of each session.

During the isometric protocol, subjects generated ramped plantar flexion contractions while we imaged the MG MTJ and tracked markers on the calcaneus and ultrasound probe (Figs. 1B and 2A). Each subject's right limb was secured in a custom frame. The frame comprised a steel foot plate that secured the ankle at one of four angles (5° dorsiflexion, 0°, 10° plantar flexion, 20° plantar flexion) and a support for the leg that fixed the knee at 130° flexion, which approximates the knee angle at 90° of the crank cycle when the AT transmits maximum force during cycling. The foot plate was instrumented with a strain gauge (Biovision, Wehrheim, Germany), and strain signals were recorded at 2000Hz. Strains were converted to torque about the ankle plantar flexion axis based on measured distances between the gauge and fulcrum of the foot plate, between the fulcrum and the foot's center of pressure (COP), and between the COP and ankle axis ( $d_G$ ,  $d_{COP}$ , and  $d_f$  respectively, Fig. 2A). The COP was estimated from a marker at the fifth metatarsal, and the ankle axis was determined from each subject's scaled model. Subjects generated three “maximal-effort” ramped contractions at each ankle angle (Suppl. Video S2).

### **Determination of Muscle Moment Arms, Muscle-Tendon Lengths and Net Ankle Moments**

We estimated the plantar flexion moment arms of the MG, LG, and SOL by scaling a musculoskeletal model to each subject (*OpenSim v3.3*, Delp et al., 2007). The model we used is based on existing models (Delp et al., 1990; Anderson and Pandy 1999; Arnold et al., 2010) and characterizes the geometry of the bones, the kinematics of the hip, knee, ankle, subtalar, and metatarsophalangeal joints, and the paths of the muscles (Fig. 1C). We constrained the paths of MG and LG to “wrap” over the posterior femoral condyles (Arnold et al., 2010), and we verified that the scaled models have plantar flexion moment arms that are similar to the moment arms (of other females) published in the literature (e.g., Sheehan, 2012 and Suppl. Table S2). We used the scaled models to estimate each subject's moment arms and MTU lengths during cycling (e.g., Suppl. Figs. S2 and S4) and during the isometric tests. We also used the models, together with the measured crank reaction forces, to calculate subjects’ net ankle moments via inverse dynamics (*OpenSim v3.3*, Delp et al.,

2007). We adjusted the mass and inertial properties of the right tibia, hind foot, and forefoot segments of the models to account for the ultrasound probe, sandals, cleats, and pedals.

### Characterization of Subject-Specific AT Force-Length Properties

We used AT forces and length changes from the isometric tests to generate a tendon force-length curve for each subject (Fig. 2). We assumed that a fraction of the plantar flexion torques measured during the isometric tests were generated by MG, LG, and SOL. To estimate this fraction, we determined the relative volumes of all the plantar flexors from regression equations (Handsfield et al., 2014), and we used each muscle's volume,  $V_m$ , together with its optimal fiber length,  $l_{f,opt}$  (from each scaled model), to estimate each muscle's physiological cross-sectional area (PCSA),  $\frac{V_m}{l_{f,opt}}$ , and maximum isometric moment-generating capacity,  $M_{m,max}$ , at joint angles corresponding to the isometric tests:

$$M_{m,max} = ma \times \left( \frac{V_m}{l_{f,opt}} \right) \sigma_0 \quad \text{Eq. (1)}$$

We assumed a specific tension,  $\sigma_0$ , of 225 kPa (Spector et al., 1980; Roy et al., 1982) and we estimated each subject's moment arms,  $ma$ , from the scaled musculoskeletal models. The combined moment-generating capacity of MG, LG, and SOL was 91% of the total and was generally consistent across joint angles and subjects (Suppl. Fig. S3). At each ankle angle tested, we calculated an “effective” plantar flexion moment arm of the AT (e.g., Biewener, 1989) by averaging the moment arms of MG, LG, and SOL weighted by their PCSAs. To generate each subject's force-length curve, we estimated each subject's AT forces from the moment arms and from 91% of the measured plantar flexion torques, and we determined the corresponding AT lengths from the ultrasound data. AT length changes and strains were determined relative to the tendon's assumed slack length. The slack length ( $l_{0AT}$ ) was estimated from cycling data, for each subject, as the AT length measured at 310° of the crank cycle, averaged over all crank cycles. This choice was motivated by *in vivo* tendon buckle data (Gregor et al., 1987) that showed AT force beginning to rise near 310° across pedaling conditions.

The AT force-length curves included a linear region and a toe region (Figs. 2B and C). We characterized the linear stiffness ( $k_{SEE}$ ) of each subject's AT by fitting a line to the linear region as force was rising (Fig. 2B). The linear stiffness did not vary with ankle angle, so we averaged values from the four angles to obtain an AT stiffness for each subject. Across subjects, AT stiffness differed significantly ( $p < 0.05$ , Fig. 2C) consistent with previous findings (Kubo et al., 2003; Lichtwark and Wilson, 2005; Muraoka et al., 2005). Within the toe region, the subjects' force-length properties could not always be resolved due to the rapid rise in force during the ramped contractions and the relatively low rate of image acquisition. However, the nonlinear stiffness was generally consistent across the four subjects for whom we could resolve these data (Suppl. Table S1). For this reason, and because strains in the toe region were small ( $1.0103\% \pm 0.22\%$ ) compared to peak strains during cycling (3-6%), we averaged the nonlinear force-length data from four subjects and used these data for all subjects (Suppl. Table 1).

### Estimation of AT Forces during Cycling

AT forces ( $F_{AT}$ ) during cycling were estimated from ultrasound-based measures of AT length ( $l_{AT}$ ) using the values of AT stiffness in the toe ( $k_{SEE,T}$ ) and linear regions ( $k_{SEE}$ ) and slack length ( $l_{0,AT}$ ) obtained for each subject:

$$F_{AT} = \begin{cases} 0, & l_{AT} \leq l_{0,AT} \\ k_{SEE,T} (l_{AT} - l_{0,AT}), & l_{0,AT} < l_{AT} \leq (l_{0,AT}) 1.0103 \\ k_{SEE} (l_{AT} - (l_{0,AT}) 1.0103) + k_{SEE,T} (l_{0,AT} (0.0101)), & (l_{0,AT}) 1.0103 < l_{AT} \end{cases} \quad (2)$$

Eq. (2)

AT stiffness was characterized based on length changes measured at the MG MTJ during ramped isometric contractions. However, the relative EMG intensities of MG, LG, and SOL – and thus the muscles' relative contributions to AT force – vary with load during cycling (Wakeling and Horn, 2009). To obtain a more representative estimate of AT force, we scaled the estimated forces  $F_{AT}$  in Eq. 2 by a factor,  $c_e$ . This factor essentially divides the measured tendon length change by the relative EMG excitation of the MG,  $\hat{e}_{MG}$ , weighted by the fractional PCSAs,  $\hat{A}_{PCSA}$ , of the MG, LG, and SOL:

$$c_e = \frac{\left( \left( \hat{e}_{MG} \hat{A}_{PCSA, MG} \right) + \left( \hat{e}_{LG} \hat{A}_{PCSA, LG} \right) + \left( \hat{e}_{SOL} \hat{A}_{PCSA, SOL} \right) \right)}{\hat{e}_{MG}} \quad \text{Eq. (3)}$$

The fractional PCSA of each muscle was calculated as the ratio of its PCSA to the summed PCSAs of the MG, LG, and SOL, which we determined from regression equations (Handsfield et al., 2014).

EMG intensities of the muscles were calculated across a 10 to 450Hz frequency band using an EMG-specific wavelet analysis (von Tscherner, 2000). EMG intensities were normalized, for each muscle, by the maximum intensity detected during the reference cycling trials. We assumed that the relative EMG intensities of the muscles during these “maximal effort” trials were similar to their intensities during the “maximal effort” isometric tests, and we assumed that EMG activity recorded on the left limb was representative of activity on the right limb shifted by 180° of the crank cycle. Because muscle force is linearly related to the EMG signal's amplitude (Milner-Brown and Stein, 1975), not its power, we calculated the square root of the mean EMG intensity as a measure of excitation for each muscle ( $\hat{e}_{MG}$ ,  $\hat{e}_{LG}$ ,  $\hat{e}_{SOL}$ ) and trial (Eq. 3).

### Evaluation of the Ultrasound-Based Method

We evaluated our procedure for estimating AT force in three ways. First, we examined whether subjects' AT forces increased with crank load as reported by Gregor et al. (1987), who analyzed *in vivo* tendon force buckle data from one subject (Gregor et al., 1987). We

used a general linear model ANOVA (*JMP* Software, SAS, Cary, USA), and we tested for the effects of load (covariate) and subject (random factor) on peak AT strain and force.

Second, we compared each subject's AT plantar flexion moments, calculated from the estimated AT forces and moment arms during cycling, to the same subject's net ankle moments from inverse dynamics (Fig. 1). In particular, we tested whether differences in these moments increased when we used the group's average AT stiffness,  $\bar{k}_{SEE}$  ( $165\text{N}\cdot\text{mm}^{-1}$  in the linear region) in Eq. 2, rather than the subject's estimated AT stiffness,  $k_{SEE}$ , or when we did not account for measured changes in the muscles' relative EMG intensities with load. To formalize these comparisons, we classified the subjects in  $2\times 2$  contingency tables and used Fisher's Exact Test. Subjects were classified based on whether their peak AT moments from ultrasound were (or were not) within  $91\pm 10\%$  of their peak moments from inverse dynamics; this criterion assumes that the MG, LG, and SOL generated about 91% of the plantar flexion moment, and the dorsiflexors were inactive (as evidenced by EMG recordings, Suppl. Fig. S1) during the downstroke.

Third, we varied each subject's AT slack length by  $\pm 1\%$  and AT stiffness by  $\pm 20\%$  and recalculated AT force for all cycling trials. This sensitivity analysis quantified how the onset and magnitude of the estimated AT forces might have been affected by errors in our subject-specific, ultrasound-based values.

## Results

Ultrasound images of the MG MTJ during cycling confirmed that the AT starts stretching during the upstroke (Fig. 3A). In the subjects tested here, the AT transmitted force between  $315^\circ\pm 5^\circ$  and  $260^\circ\pm 10^\circ$  of the crank cycle, reaching maximum force at  $100^\circ\pm 15^\circ$  of the crank cycle. Peak AT strains increased with load in all subjects ( $p<0.05$ ). On average, peak strains were 3% (range: 2-4.7%) at the lowest load and more than 5% (range: 4-7.3%) at the highest load (Fig. 3B). By contrast, subjects' knee and ankle angles and associated MTU lengths were highly constrained across loads (Suppl. Fig. S4).

Subjects' estimated AT forces (Fig. 4) and the normalized EMG intensities of the MG, LG, and SOL (Fig. 5) also increased with load ( $p<0.05$ ). These trends are consistent with the previous tendon buckle study by Gregor et al. (1991) and with EMG data published in the literature (e.g., Ericson et al., 1984; Baum and Li, 2003; Wakeling and Horn, 2009). Subjects' peak AT forces during cycling averaged 920N (range: 410-1225N) at the lowest load and 1510N (range: 650-2180N) at the highest load (Fig. 4). At the highest load (44N·m, 370W), the peak forces represented 30 to 50% of the combined MG, LG, and SOL muscles' maximum isometric force-generating capacity. Increases in the EMG intensities of MG, LG, and SOL were generally consistent with the timing of increases in AT force (Fig. 5). By contrast, the TA was not active during the downstroke (Suppl. Fig. S1).

Plantar flexion moments, derived from the estimated AT forces, reproduced the temporal patterns of each subject's net ankle moments calculated from inverse dynamics (e.g., Fig. 6 and Suppl. Fig. S5). Subjects' peak AT moments were less than their net ankle moments in

most cases (Fig. 7, black bars); on average, the AT moments were 12% less at the lowest load and 5% less at the highest load during the downstroke.

Differences between subjects' AT moments and net ankle moments increased substantially when we did not account for changes in the muscles' relative EMG intensities with load (i.e., when we neglected scale factor  $c_e$ ) or, for some subjects, when we used an average AT stiffness rather than the subject's estimated value (Fig. 7). Three subjects, for example, had tendons that were substantially more compliant than the average (i.e.,  $k_{SEE} < \bar{k}_{SEE}$  by  $15\text{N}\cdot\text{mm}^{-1}$  or more). In these cases, using the average stiffness in Eq. 2 overestimated AT force (Fig. 7A). All ten subjects showed variations in the muscles' EMG patterns at the different crank loads (Fig. 5D). Typically, the normalized EMG intensities of the three plantar flexors were similar at the high load, but the intensity of SOL was proportionally decreased at the low load. When we did not account for these changes, our procedure overestimated AT force, especially at the low loads (Fig. 7B).

## Discussion

This study evaluated a procedure for estimating *in vivo* AT forces from ultrasound images. Comprehensive data sets from ten elite cyclists were used to test two approaches: (i) accounting for subject-specific AT stiffness and (ii) accounting for changes in the relative EMG intensities of the MG, LG, and SOL. Our analyses show that length changes of the AT, determined from tracking the MG MTJ, can provide estimates of subjects' AT forces and moments that are consistent with the subjects' net ankle moments calculated from inverse dynamics – but only when the muscles' relative EMG intensities are considered. Other investigators have speculated that the muscles' activity should be considered (e.g., Gregor et al., 1991; Farris and Sawicki, 2012), and our study provides new evidence that this is indeed the case.

Rigorous evaluation of the estimated AT forces is challenging. Here, we used subjects' net ankle moments from inverse dynamics as a check, and we assumed that the triceps surae could generate at most 91% of the plantar flexion moment. In 9 of 10 subjects, across all load conditions, the peak AT moments – estimated from Eq. 2, Eq. 3, and each subject's scaled model – were within  $91\pm 10\%$  of the peak moment calculated from inverse dynamics. Fewer subjects met this criterion when we used an average stiffness to estimate AT force (4 of 10 subjects,  $p<0.01$ , Fig. 7A), and even fewer subjects met this criterion when we neglected the EMG-based scale factor  $c_e$  (1 of 10 subjects,  $p<0.01$ , Fig. 7B).

Even with these refinements, the AT moments for four subjects were equal to or greater than the inverse dynamics-based moments. It is likely that AT forces were overestimated in these cases, and there are several possible explanations. First, co-contraction of the TA or other dorsiflexors may have decreased the net moment calculated from inverse dynamics. Our EMG data show that the TA was active from approximately  $260^\circ$  to  $360^\circ$  of the crank cycle, and this may explain a portion of the discrepancy near top dead center when AT force was rising, particularly at the highest load (Fig. 6B). However, the TA was not active during the downstroke (Suppl. Fig. S1), and our subjects' net ankle moments were within ranges

reported in the literature for comparable cadences and loads (Gregor et al., 1985; Hull and Jorge, 1985; Smak et al., 1999).

Second, we may have overestimated the effective moment arm of the AT the ankle. We scaled a generic model to each subject based on markers at the lateral malleolus and calcaneus, and these markers tracked well during cycling. However, we did not measure subjects' AT moment arms. If we overestimated subjects' moment arms, then our estimates of AT force may be better than our estimates of AT moments.

Third, we may have overestimated AT stiffness during the isometric tests if muscles other than MG, LG, or SOL made substantial contributions to the measured plantar flexion torque (i.e., more than 9%), or if we overestimated the distance between the ankle's axis of rotation and the foot's center of pressure ( $d_f$  in Fig. 2A). We did not record EMG data during the isometric tests, nor did we precisely measure the center of pressure, so we cannot assess these explanations. However, the average AT stiffness that we measured ( $165\text{N}\cdot\text{mm}^{-1}$ ) is between values commonly cited in the literature ( $150$  to  $190\text{N}\cdot\text{mm}^{-1}$ , Maganaris and Paul, 2002; Lichtwark and Wilson, 2005). Changing AT stiffness by  $\pm 10\%$  altered the estimated AT force by  $\pm 10\%$  of the muscles' maximum isometric force (Suppl. Fig. S6); thus, subject-specific errors in AT stiffness could explain the discrepancies observed.

Fourth, we may have underestimated AT slack length. In our sensitivity study, small increases in slack length substantially delayed the onset of AT force during the upstroke (Suppl. Fig. S6A), yet the timing of our subjects' estimated AT moments were generally consistent with the timing of their net moments, particularly at low loads when there was minimal co-contraction (e.g., Fig. 6A and Suppl. Fig. S1). Thus, we are reasonably confident in the AT slack lengths that we measured, which were based on observations from Gregor et al. (1987). We are less confident in our estimate of AT length at the transition between the toe region and the linear region; if we underestimated toe region strain, then it is plausible that we over-estimated AT force in the linear region.

Lastly, we characterized force-length properties of the AT at only one knee angle, and we measured length changes only at the MG MTJ. However, forces transmitted by the AT depend on the excitations and length changes of the MG, LG, and SOL. We scaled the estimated forces (Eq. 2) by a factor ( $c_e$ , Eq. 3) to account for changes in the muscles' relative EMG intensities with load – but we did not characterize the non-uniform strains within the AT during cycling (e.g., Franz et al. 2015) that result, in part, from the muscles' force-length properties and the fact that the MG and LG, but not the SOL, cross the knee. Hence, our mapping from AT strain to force (Fig. 2) may have under-estimated force when the knee was flexed more than it was during the isometric test (i.e., near top dead center), and it may have over-estimated force when the knee was flexed less than it was during the isometric test (i.e., near bottom dead center). Without the EMG scale factor, subjects' AT forces were consistently over-estimated (Fig. 7), particularly at low loads when SOL was less active (Fig. 5C). To further improve the accuracy of AT forces estimated from ultrasound-based AT strains, these length-dependent effects may need to be considered.

The peak AT forces that we estimated during cycling (range: 410-2180N across 10 subjects and 4 loads) are generally greater than the forces measured by Gregor et al. (1987) (range: 480-661N across 3 loads) – though there is overlap in the forces at low loads, and our subjects' net moments at these loads (Suppl. Fig. S7) are similar to those that Gregor et al. reported (1991). Differences in the forces may be related to the invasive nature of tendon buckle experiments (Gregor et al., 1987; Gregor et al., 1991) or to differences in the subjects' muscular capacities that influenced their pedaling strategies. Regardless, our study is the first to confirm non-invasively several of the findings reported by Gregor et al. (1987, 1991). For example, we showed that AT force increases with load, consistent with tendon buckle data.

In closing, traditional motion analysis provides information about joint motions during movement, but provides limited insight into muscle-tendon mechanics. Hill-type muscle models are increasingly being used within simulations to infer the forces that cause measured motions (e.g. Anderson and Pandy, 2003; Hamner et al., 2011; Kautz and Neptune, 2002), but these predictions are rarely tested against independent measures, such as muscle and tendon length changes or forces estimated *in vivo*. Tendon buckle transducers have been used to quantify *in vivo* forces, but remain impractical for most human applications. The ultrasound-based procedure described in this study augments existing methods and is applicable to studies of muscle-tendon mechanics and tests of muscle-driven simulations.

## Supplementary Material

Refer to Web version on PubMed Central for supplementary material.

## Acknowledgements

We thank Dr. Andrew Biewener for valuable feedback and Sidney Morrison for assistance during data collection. We gratefully acknowledge funding from NIH Grant R01 2R01AR055648 and an NSERC Graduate Research Fellowship to T.J.M. Dick.

## References

1. Anderson FC, Pandy MG. A dynamic optimization solution for vertical jumping in three dimensions. *Comp. Meth. Biomech. Biomed. Eng.* 1999; 2:201–231.
2. Anderson FC, Pandy MG. Individual muscle contributions to support in normal walking. *Gait Posture.* 2003; 17:159–69. [PubMed: 12633777]
3. Arnold EM, Ward SR, Lieber RL, Delp SL. A model of the lower limb for analysis of human movement. *Ann. Biomed. Eng.* 2010; 38:269–279. [PubMed: 19957039]
4. Baum BS, Li L. Lower extremity muscle activities during cycling are influenced by load and frequency. *J. Electromyogr. Kinesiol.* 2003; 13:181–190. [PubMed: 12586523]
5. Biewener AA. Scaling body support in mammals: limb posture and muscle mechanics. *Science.* 1989; 245:45–48. [PubMed: 2740914]
6. Blake OM, Wakeling JM. Muscle coordination limits efficiency and power output of human limb movement under a wide range of mechanical demands. *J. Neurophysiol.* 2015; 114:3283–3295. [PubMed: 26445873]
7. Delp SL, Loan JP, Hoy MG, Zajac FE, Topp EL, Rosen JM. An interactive graphics-based model of the lower extremity to study orthopaedic surgical procedures. *IEEE Trans. Biomed. Eng.* 1990; 37:757–767. [PubMed: 2210784]

8. Delp SL, Anderson FC, Arnold AS, Loan P, Habib A, John CT, Thelen DG. OpenSim: open-source software to create and analyze dynamic simulations of movement. *IEEE Trans. Biomed. Eng.* 2007; 54:1940–1950. [PubMed: 18018689]
9. Ericson MO, Nisell R, Arborelius UP, Ekholm J. Muscular activity during ergometer cycling. *Scand. J. Rehab. Med.* 1984; 17:53–61.
10. Farris DJ, Sawicki GS. Human medial gastrocnemius force–velocity behaviour shifts with locomotion speed and gait. *Proc. Nat. Acad. Sci.* 2012; 109:977–982. [PubMed: 22219360]
11. Franz JR, Slane LC, Rasske K, Thelen DG. Non-uniform in vivo deformations of the human Achilles tendon during walking. *Gait Posture.* 2015; 41:192–197. [PubMed: 25457482]
12. Gregor RJ, Cavanagh PR, LaFortune M. Knee flexor moments during propulsion in cycling—A creative solution to Lombard's Paradox. *J. Biomech.* 1985; 18:307–316. [PubMed: 4008501]
13. Gregor RJ, Komi PV, Järvinen M. Achilles tendon forces during cycling. *Int. J. Sports Med.* 1987; 8:9–14. [PubMed: 3583522]
14. Gregor RJ, Komi PV, Browning RC, Järvinen M. A comparison of the triceps surae and residual muscle moments at the ankle during cycling. *J. Biomech.* 1991; 24:287–297. [PubMed: 2050705]
15. Hamner SR, Seth A, Delp SL. Muscle contributions to propulsion and support during running. *J. Biomech.* 43:2709.
16. Handsfield GG, Meyer CH, Hart JM, Abel MF, Blemker SS. Relationships of 35 lower limb muscles to height and body mass quantified using MRI. *J. Biomech.* 2014; 47:631–638. [PubMed: 24368144]
17. Hashizume S, Iwanuma S, Akagi R, Kanehisa H, Kawakami Y, Yanai T. In vivo determination of the Achilles tendon moment arm in three-dimensions. *J. Biomech.* 2012; 45:409–413. [PubMed: 22055426]
18. Hull ML, Jorge M. A method for biomechanical analysis of bicycle pedalling. *J. Biomech.* 1985; 18:631–644. [PubMed: 4077861]
19. Kautz SA, Neptune RR. Biomechanical determinants of pedalling energetics: internal and external work are not independent. *Exer. Sport Sci. Rev.* 2002; 30:159–65.
20. Kongsgaard M, Nielsen CH, Hegnsvad S, Aagaard P, Magnusson SP. Mechanical properties of the human Achilles tendon, in vivo. *Clin. Biomech.* 2011; 26:772–777.
21. Kubo K, Kanehisa H, Fukunaga T. Gender differences in the viscoelastic properties of tendon structures. *Eur. J. Appl. Physiol.* 2003; 88:520–526. [PubMed: 12560950]
22. Kurokawa S, Fukunaga T, Fukashiro S. Behaviour of fascicles and tendinous structures of human gastrocnemius during vertical jumping. *J. Appl. Physiol.* 2001; 90:1349–1358. [PubMed: 11247934]
23. Lee SS, Piazza SJ. Built for speed: musculoskeletal structure and sprinting ability. *J. Exp. Biol.* 2009; 212:3700–3707. [PubMed: 19880732]
24. Lichtwark GA, Wilson AM. In vivo mechanical properties of the human Achilles tendon during one-legged hopping. *J. Exp. Biol.* 2005; 208:4715–4725. [PubMed: 16326953]
25. Lichtwark GA, Wilson AM. Interactions between the human gastrocnemius muscle and the Achilles tendon during incline, level and decline locomotion. *J. Exp. Biol.* 2006; 209:4379–4388. [PubMed: 17050853]
26. Maganaris CN, Baltzopoulos V, Sargeant AJ. Changes in Achilles tendon moment arm from rest to maximum isometric plantar flexion: in vivo observations in man. *J. Physiol.* 1998; 510:977–985. [PubMed: 9660906]
27. Maganaris CN, Paul JP. In vivo human tendon mechanical properties. *J. Physiol.* 1999; 521:307–313. [PubMed: 10562354]
28. Maganaris CN, Paul JP. Tensile properties of the in vivo human gastrocnemius tendon. *J. Biomech.* 2002; 35:1639–1646. [PubMed: 12445617]
29. Maganaris CN. Force-length characteristics of the in vivo human gastrocnemius muscle. *Clin. Anat.* 2003; 16:215–223. [PubMed: 12673816]
30. Magnusson SP, Aagaard P, Rosager S, Dyhre-Poulsen P, Kjaer M. Load-displacement properties of the human triceps surae aponeurosis in vivo. *J. Physiol.* 2001; 531:277–288. [PubMed: 11179410]

31. Milner-Brown HS, Stein RB. The relation between the surface electromyogram and muscular force. *J. Physiol.* 1975; 246(3):549. [PubMed: 1133787]
32. Morrison SM, Dick TJ, Wakeling JM. Structural and mechanical properties of the human Achilles tendon: Sex and strength effects. *J. Biomech.* 2015 doi:10.1016/j.jbiomech.2015.06.009.
33. Muramatsu T, Muraoka T, Takeshita D, Kawakami Y, Hirano Y, Fukunaga T. Mechanical properties of tendon and aponeurosis of human gastrocnemius muscle in vivo. *J. Appl. Physiol.* 2001; 90:1671–1678. [PubMed: 11299254]
34. Muraoka T, Muramatsu T, Fukunaga T, Kanehisa H. Elastic properties of human Achilles tendon are correlated to muscle strength. *J. Appl. Physiol.* 2005; 99:665–669. [PubMed: 15790689]
35. Prager RW, Rohling RN, Gee AH, Berman L. Rapid calibration for 3-D freehand ultrasound. *Ultrasound Med. Biol.* 1998; 24:855–869. [PubMed: 9740387]
36. Rouffet DM, Hautier CA. EMG normalization to study muscle activation in cycling. *J. Electromyogr. Kinesiol.* 2008; 18:866–878. [PubMed: 17507240]
37. Roy RR, Meadows ID, Baldwin KM, Edgerton VR. Functional significance of compensatory overloaded rat fast muscle. *J. Appl. Physiol.* 1982; 52:473–478. [PubMed: 7061301]
38. Rugg SG, Gregor RJ, Mandelbaum BR, Chiu L. In vivo moment arm calculations at the ankle using magnetic resonance imaging (MRI). *J. Biomech.* 1990; 23:495499–497501.
39. Sheehan FT. The 3D in vivo Achilles' tendon moment arm, quantified during active muscle control and compared across sexes. *J. Biomech.* 2012; 45:225–230. [PubMed: 22138193]
40. Siston RA, Delp SL. Evaluation of a new algorithm to determine the hip joint center. *J. Biomech.* 2006; 39:125–130. [PubMed: 16271596]
41. Smak W, Neptune RR, Hull ML. The influence of pedaling rate on bilateral asymmetry in cycling. *J. Biomech.* 1999; 32:899–906. [PubMed: 10460126]
42. Spector SA, Gardiner PF, Zernicke RF, Roy RR, Edgerton VR. Muscle architecture and force-velocity characteristics of cat soleus and medial gastrocnemius: implications for motor control. *J. Neurophysiol.* 1980; 44:951–960. [PubMed: 7441324]
43. von Tscharnner V. Intensity analysis in time-frequency space of surface myoelectric signals by wavelets of specified resolution. *J. Electromyogr. Kinesiol.* 2000; 10:433–445. [PubMed: 11102846]
44. Wakeling JM, Horn T. Neuromechanics of muscle synergies during cycling. *J. Neurophysiol.* 2009; 101:843–854. [PubMed: 19073812]
45. Wakeling JM, Blake OM, Chan HK. Muscle coordination is key to the power output and mechanical efficiency of limb movements. *J. Exp. Biol.* 2010; 213:487–492. [PubMed: 20086134]
46. Wolf SL, Ammerman J, Jann B. Organization of responses in human lateral gastrocnemius muscle to specified body perturbations. *J. Electromyogr. Kinesiol.* 1998; 8:11–21. [PubMed: 9667030]

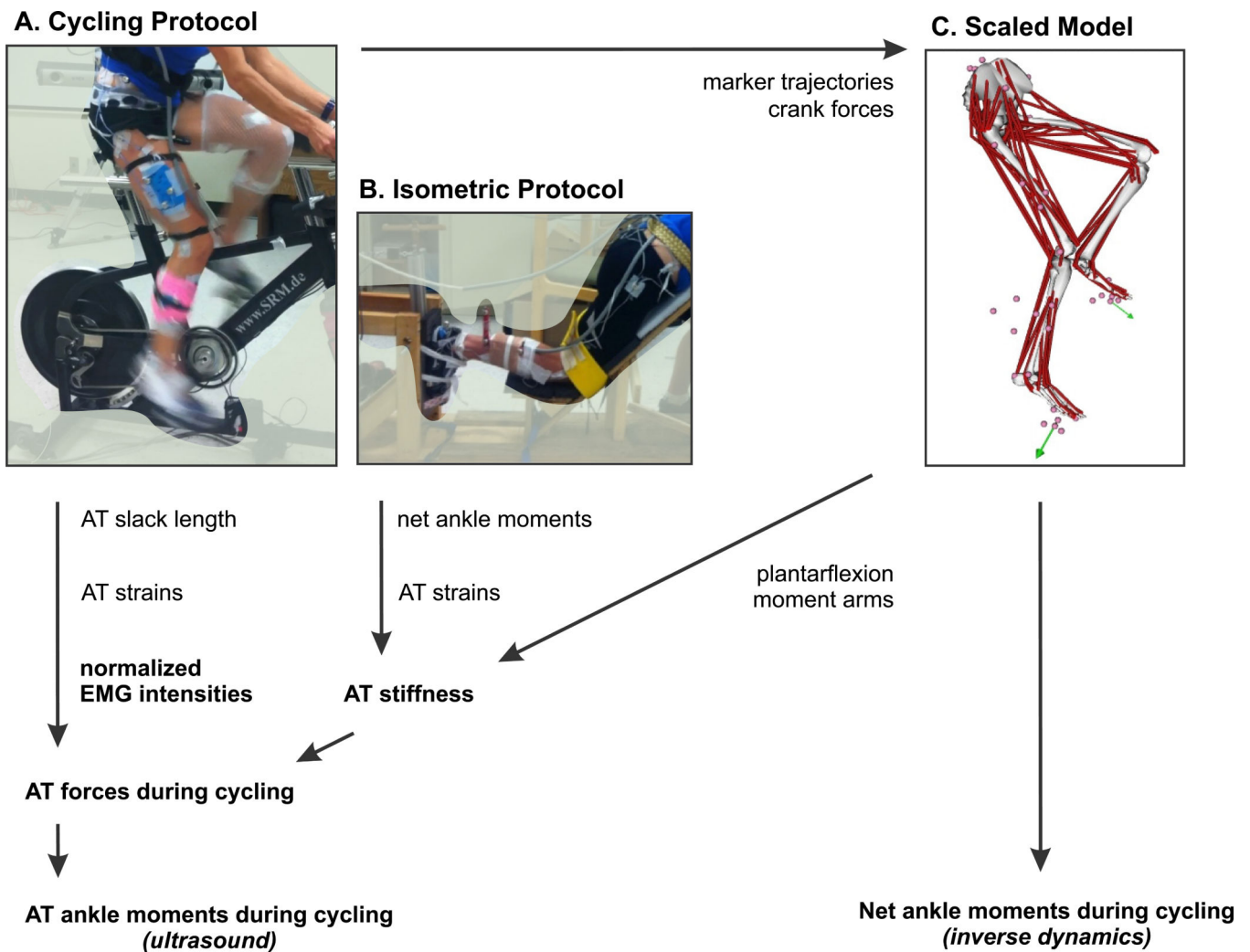
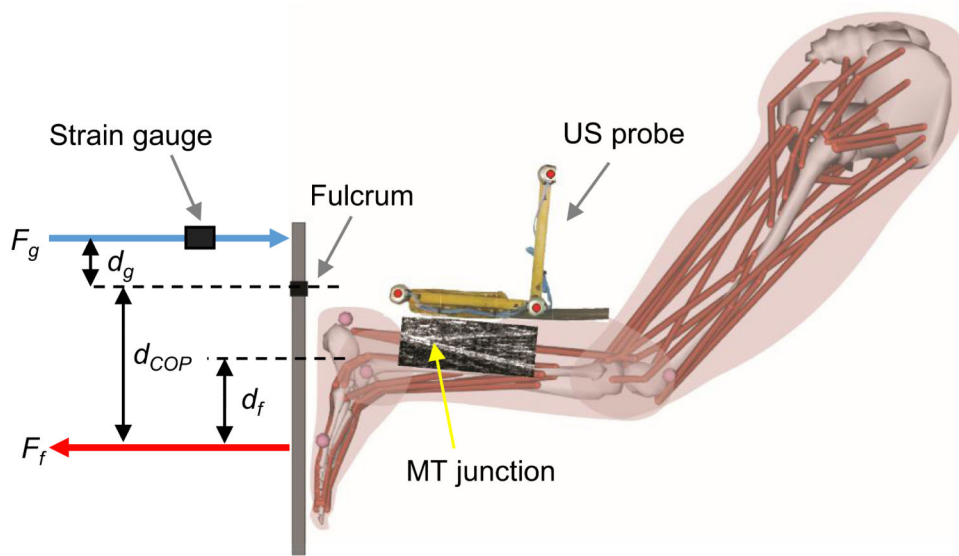


**Fig 1.** Approach for estimating and evaluating *in vivo* Achilles tendon (AT) forces during cycling from tracked ultrasound images. During the cycling protocol (A), subjects pedaled on a stationary bike while we measured AT length changes, 3D marker trajectories, crank reaction forces, and surface EMG. A trigger from the ultrasound system was used to synchronize all data, and we confirmed synchronization by identifying the start of each crank cycle from markers on the left pedal. During the isometric protocol (B), subjects generated ramped plantar flexion contractions while we measured AT length changes and plantar flexion torques; these data were used to estimate AT stiffness. A musculoskeletal model (C) was scaled to each subject and was used to calculate the muscles' plantar flexion moment arms and net ankle moments during cycling. For each subject, we compared ankle moments derived from the AT forces (left) to the net ankle moments calculated via inverse dynamics (right). We examined whether the AT moments changed when we used an average stiffness, rather than the measured stiffness, or when we neglected to account for relative differences in the EMG intensities of the triceps surae muscles. Experimental data from a representative subject are provided in Supplementary Materials (Suppl. Fig. S1).

**A.**



**B. AT stiffness at 4 ankle angles**

**C. AT force-strain behaviour for 10 subjects**

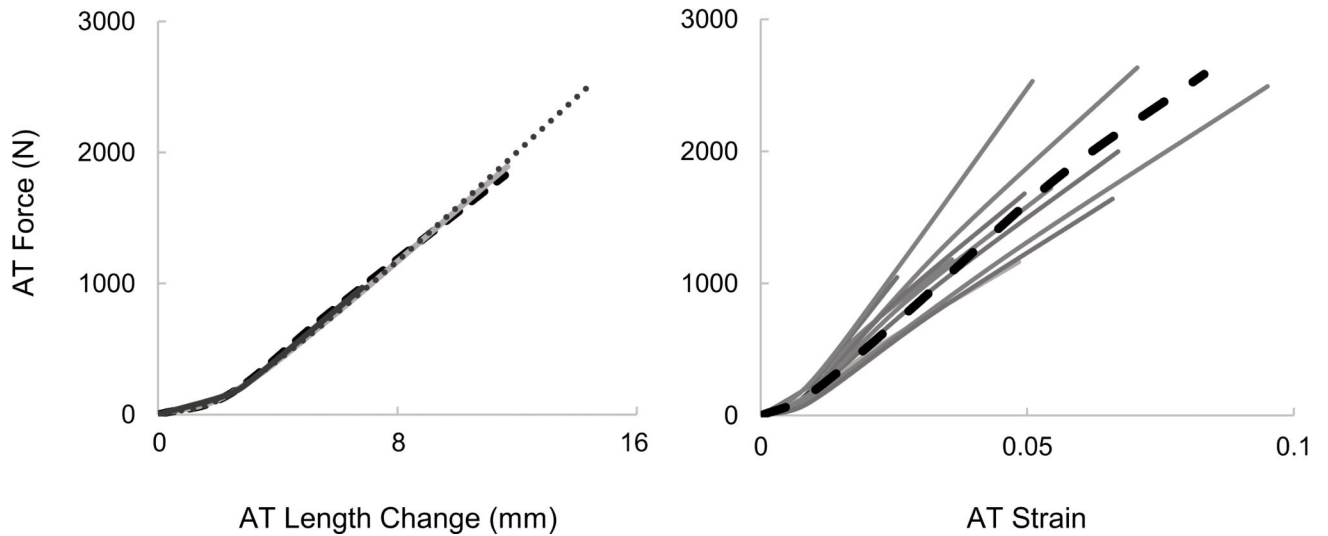


**Fig 2.**

Procedure for measuring Achilles tendon (AT) stiffness in individual subjects. Forces transmitted by the AT during ramped isometric contractions were estimated based on measurements of plantar flexion torque, obtained from an instrumented foot plate with known geometry (Morrison et al. 2015), and plantar flexion moment arms, calculated from a scaled musculoskeletal model (A); 91% of the measured moment was assumed to be transmitted by the tendon. The corresponding AT length changes were measured from tracked ultrasound images. We identified the distal MG MTJ manually in each image

(ImageJ, NIH, Maryland, USA) as the intersection between the most distal part of the muscle and the external tendon. For each ankle angle tested, a line was fit to the linear region of the force versus length change data, and these slopes were averaged (e.g., thin dotted line) to obtain AT stiffness (B). Subjects' AT forces during cycling were determined two ways: using the measured AT stiffness, and using the group's average stiffness (thick dotted line, C). To visually make comparisons across subjects, AT length changes were converted to AT strains (shown here) by dividing by AT slack length. AT stiffness values for all subjects are provided in Supplementary Materials (Suppl. Table S1), along with sample ultrasound video (Suppl. Video S1).

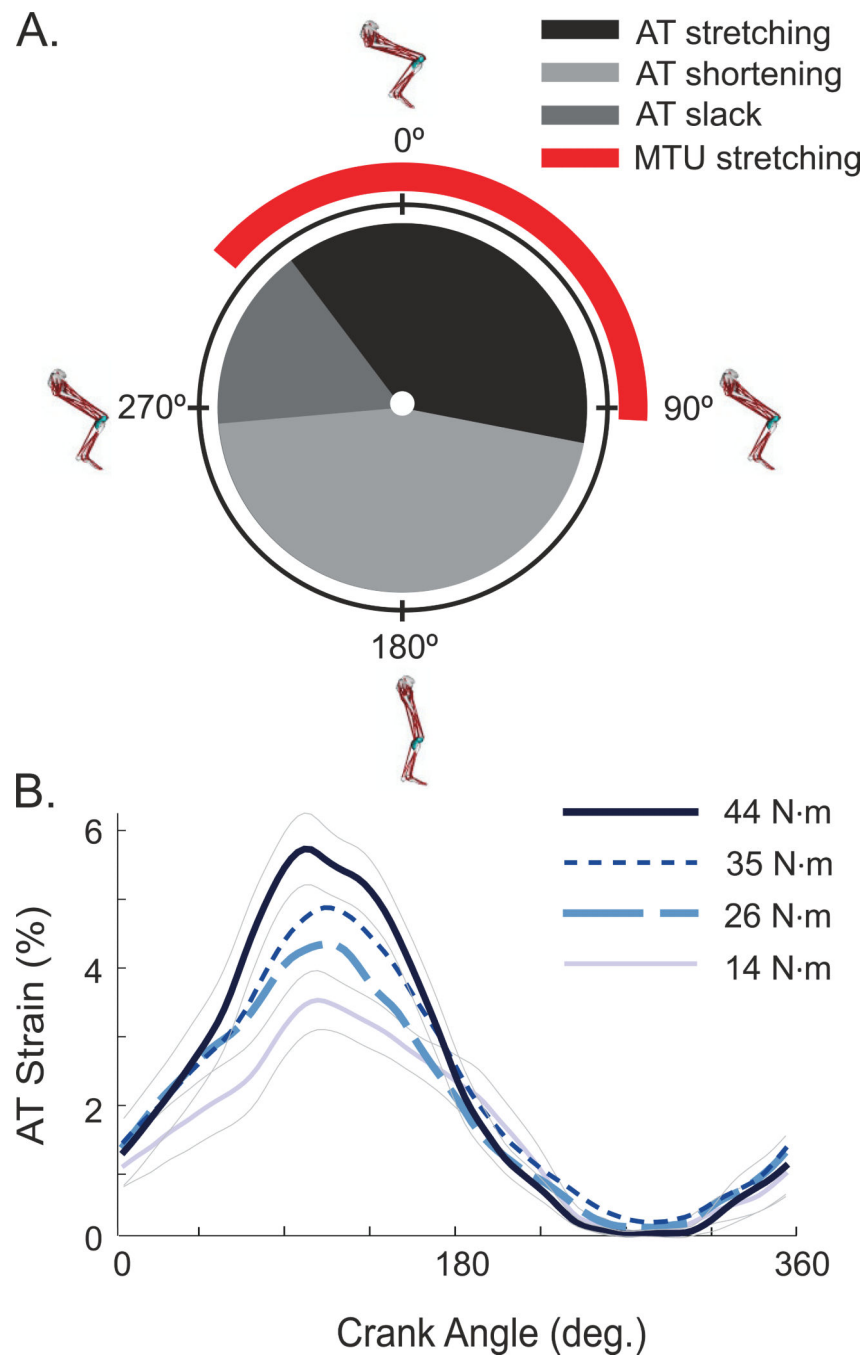


**Fig 3.** Variation in AT strain during the crank cycle (A) and across 4 crank loads (B). The tendon stretches from 315° to 100° of the crank cycle (black), shortens through 180° (light grey), and shortens below its slack length at 215° (dark grey). Time-varying AT strains during cycling (B) are presented as mean  $\pm$  SE for 10 subjects at 4 crank loads, corresponding to crank powers of 115, 220, 290, and 370 W. Thin grey curves represent the SE and are shown for the low and high loads; SE values were similar across all loads. Sample ultrasound video is provided in Supplementary Materials (Suppl. Video S2).

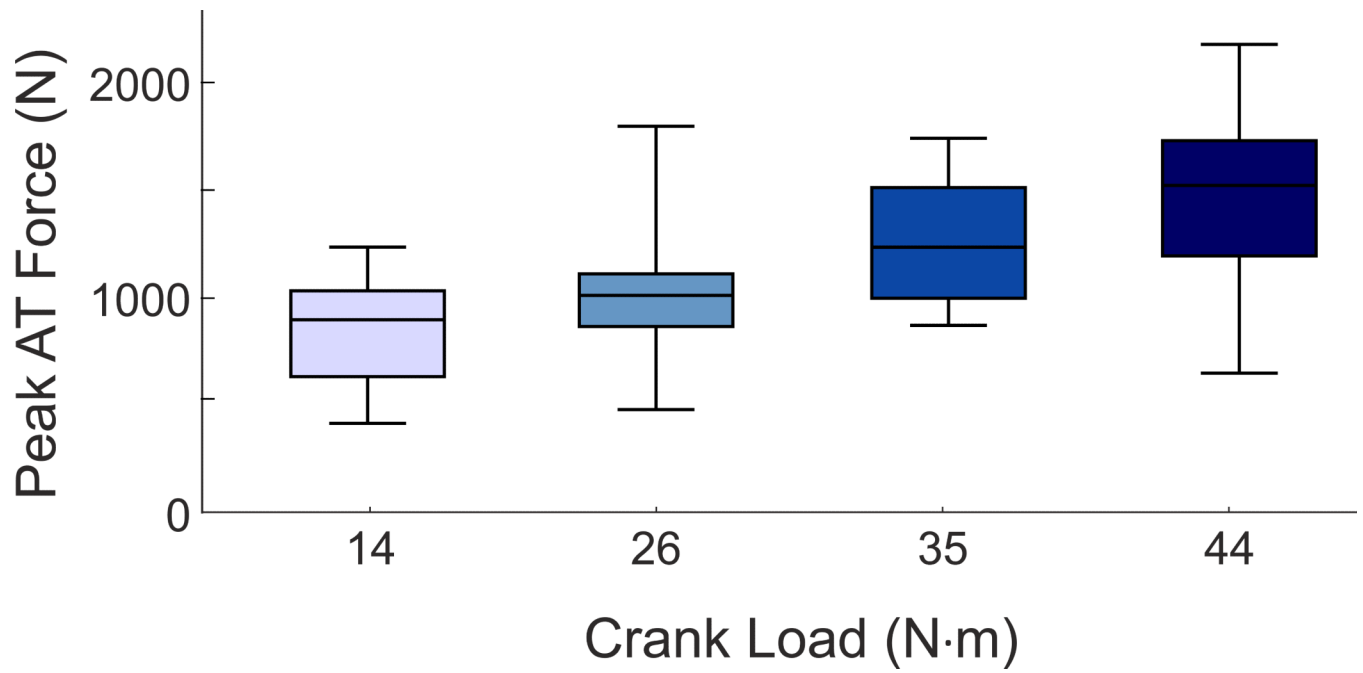


**Fig 4.** Increase in AT force with crank load. Peak AT forces are shown as box and whisker plots (median, interquartile range, range) for 10 subjects cycling at 80 r.p.m. at 4 crank loads, corresponding to crank powers of 115, 220, 290, and 370 W.

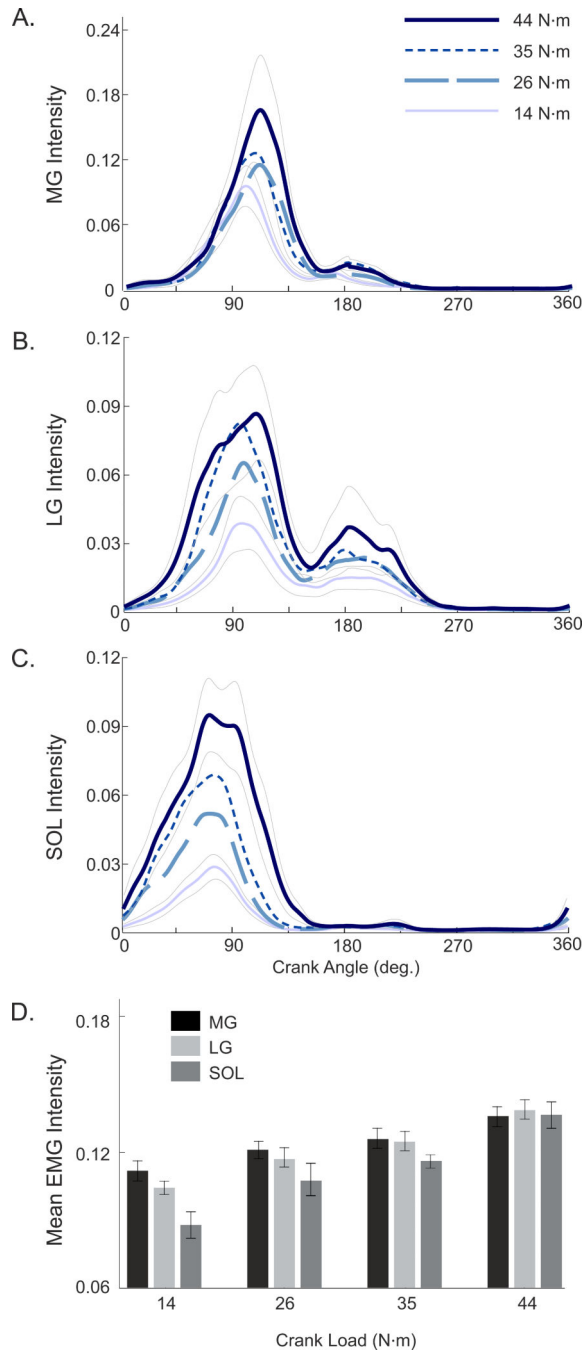


**Fig 5.** Normalized EMG intensities of the medial gastrocnemius (MG, A), lateral gastrocnemius (LG, B), and soleus (SOL, C) during cycling at 80 r.p.m. at 4 different loads, averaged across 10 subjects. Thin grey curves represent the SE and are shown for the low and high loads; SE values were similar across all loads. Relative intensities of MG, LG, and SOL during cycling vary with load (D). EMG intensity is normalized to muscle-specific maximum values collected during “maximum effort” reference cycling trials. Bars represent mean  $\pm$  SE.

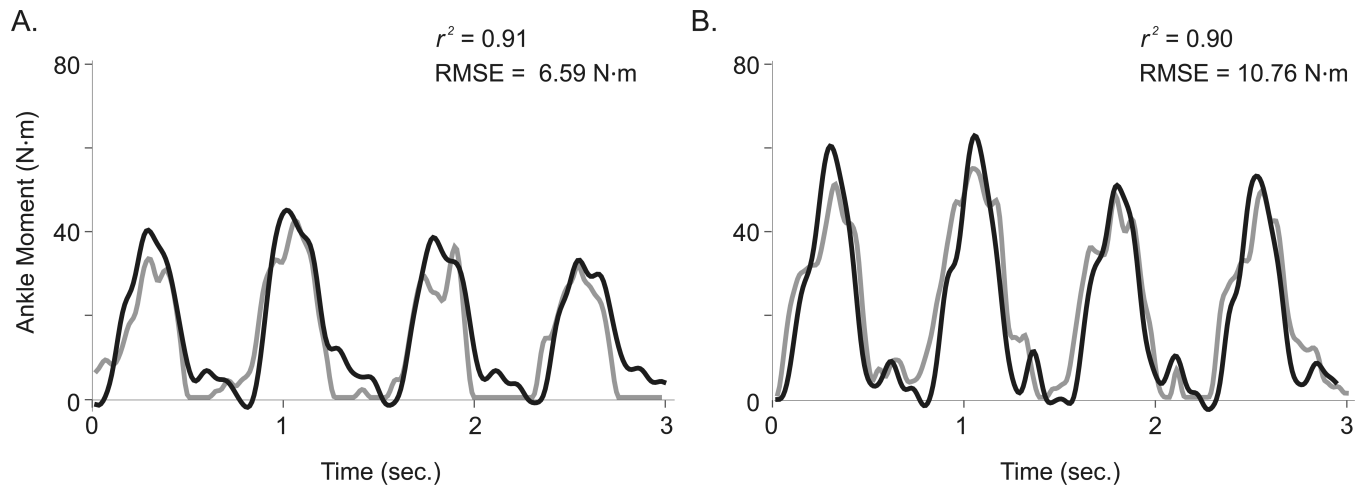


**Fig. 6.** Comparison of AT plantar flexion moments (from ultrasound-based measures of AT strains, grey) and net ankle moments (from inverse dynamics, black) for a representative subject pedaling at 80 r.p.m. at crank loads of 26 N·m (220 W, A) and 44 N·m (370 W, B). Additional comparisons, averaged across subjects, are provided in Supplementary Materials (Suppl. Fig. 4).

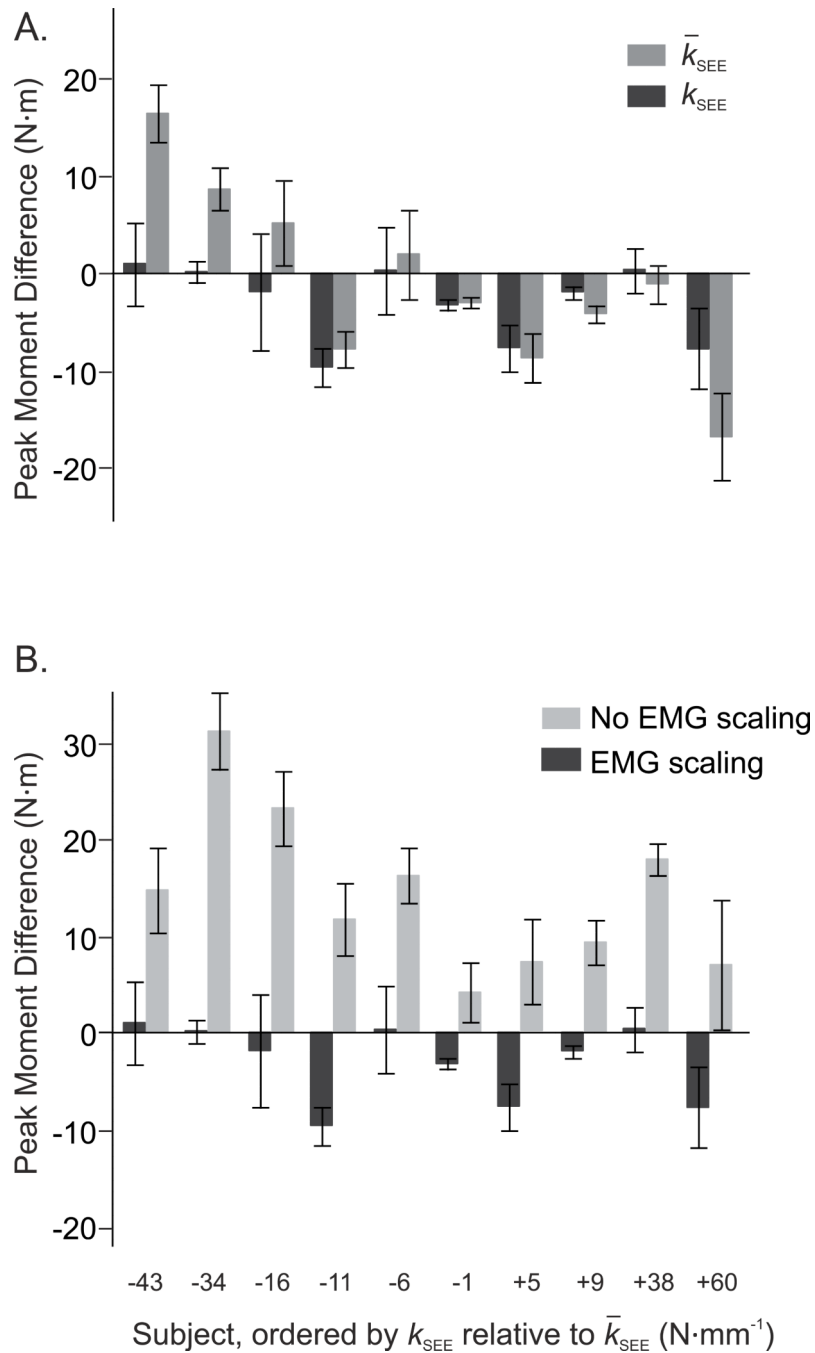


**Fig. 7.** Effects of two methodological refinements on estimated AT ankle moments: accounting for subject-specific variations in AT stiffness (A) and accounting for relative changes in the EMG intensities of MG, LG, and SOL (B). Each pair of bars shows the difference between the peak AT moment (from ultrasound) and the peak net ankle moment (from inverse dynamics) for a single subject during cycling, averaged across four loads (mean  $\pm$  SE). A negative value indicates that the ultrasound-based moment was less than the net moment (as expected if plantar flexors in addition to MG, LG, and SOL were active during the

downstroke). Subjects are ordered by their estimated AT stiffness ( $k_{SEE}$ ) relative to the group's average AT stiffness ( $\bar{k}_{SEE}$ ); subjects with negative values had more compliant tendons than the average, and subjects with positive values had stiffer tendons than the average. When subject-specific stiffness, together with an EMG scale factor that accounted for the muscles' relative EMG intensities, was used to estimate AT moment (black bars), the resulting estimates were usually better than when moments were calculated using the group's average stiffness ( $\bar{k}_{SEE}$ , dark grey bars, A) or when moments were calculated without accounting for the muscles' relative EMG intensities (light grey bars, B).